2016/08/11
Head Id: 364406
Archive Id: 364411
Archive Date: 2016/08/11
Archive Tag: trunk

Measurements of the charm jet cross-section and nuclear modification in pPb collisions at $\sqrt{s_{NN}}$=5.02 TeV

The CMS Collaboration

Abstract

We present the first measurement of jets from charm quarks ~~in a~~ produced in proton-lead ~~collision system~~(pPb) collisions at a nucleon-nucleon center of mass energy of $\sqrt{s_{NN}}$ = 5.02 TeV, as well as ~~additional~~ results from charm quark jets in proton-proton ~~collisions~~(pp) collisions at $\sqrt{s}$ = 2.76 and 5.02 TeV. By comparing the ~~charm jet~~ yield between the proton-lead and proton-proton collision systems at the same energy, we observe that the jet energy modification in proton-lead collisions (R_{pA}) at $\sqrt{s_{NN}}$ = 5.02 TeV is 0.951 $\pm$ 0.139 (stat+syst) $\pm$ 0.04 (lumi). This is consistent with an absence of final-state energy loss ~~effects~~ for charm quarks in proton-lead collisions, as expected in pQCD model predictions. In addition, we observe that the charm jet fraction is consistent with that predicted by PYTHIA to within systematic uncertainties for both proton-proton collisions at $\sqrt{s}$ = 2.76 and 5.02 TeV, as well as in proton-lead collisions at a center-of-mass energy of $\sqrt{s_{NN}}$ = 5.02 TeV.

1 Introduction

By colliding heavy nuclei at the Large Hadron Collider (LHC), one expects to reach sufficiently large energy densities to form a quark-gluon plasma (QGP), a state which is characterized by an effective deconfinement of the color degrees of freedom. Hard-scattered partons are expected to suffer energy loss as they traverse the QGP via elastic and inelastic interactions [1]. This is commonly thought to be the mechanism responsible for the observed suppression of high transverse momentum (p_{T}) hadrons and jets, or "jet quenching", in nuclear collisions.

Measurements from proton-lead (pPb) collisions allow for the factorization of ~~the~~ any initial state "cold nuclear matter" effects from the suppression effects ~~observed~~ due to the dense medium created in collisions of heavier nuclei [2]. ~~These measurements are especially crucial in light of the results of the inclusive charged particle measurement , which shows that charged hadrons in pPb collisions show an intriguing enhancement at very large values of track . Studies of jets in pPb, however, observe no such enhancement . These previous results, however, use interpolations of pp data to obtain a reference measurement at 5.02 TeV, while this analysis uses a true pp reference from 5.02 TeV data, which has only recently been collected at the LHC. Use of a non-interpolated pp reference should disentangle some of these somewhat conflicting results.~~

The jet quenching in ~~heavy-ion~~ heavy ion collisions is expected to depend upon the flavor of the fragmenting parton, primarily due to two effects. First, ~~there are significant differences in the quark and gluon jet fractions between measurements of inclusive jets and those of jets~~ jets from heavy quarks do not contain any gluon-jet component, contrary to a measurement of inclusive jets [3, 4]~~and second, quark mass effects ought to affect the interplay between various energy loss mechanisms~~. Under the assumption that gluon radiation is the dominant mechanism for energy loss, gluon jets are expected to quench more strongly than quark jets, owing to the larger color factor for gluon emission from gluons than from quarks [5]. By identifying charm (c jets) and bottom jets (b jets), measurements can be performed on a jet sample ~~dominated by~~ exclusively made up of quark jets.

In addition, ~~heavy-flavor~~ heavy quark jets may have mass-dependent effects further separating their energy loss measurements from those of inclusive jets. For example, it is expected that the radiative and collisional energy loss mechanisms should have relatively different strengths between heavy quark and light quark jets [6]. ~~Because of these effects, it is important to measure these nuclear modification effects as a function of flavor, as these can place powerful constraints on~~ Measurements of heavy quark jets, therefore, can shed light on the relative importance of these various energy loss mechanisms~~in the hot and dense medium in heavy-ion collisions, while additionally constraining nuclear initial-state effects in proton-nucleus collisions~~. While b jets have been analyzed previously [7, 8], c jets have never been explicitly measured in collisions of any particles other than protons. In addition, while the modification factor R_{pA} for both charged particles [9] and inclusive jets [10] at $\sqrt{s_{NN}}$ = 5.02 TeV have been presented, these have not yet used 5.02 TeV proton-proton (pp) data as a reference.

We present here the first measurement of c jet cross-sections and c jet fractions in a heavy ion environment in ~~proton-lead (pPb) collisions at~~ pPb collisions at $\sqrt{s_{NN}}$ = 5.02 TeV as well as in ~~proton-proton (pp)~~ pp collisions at 2.76 TeV and 5.02 TeV. Charm jets are selected by tagging on displaced secondary vertices with at least three associated tracks. ~~Then, the sample purity is found by fitting flavor contributions from simulated templates of a quantity known as the corrected secondary vertex mass to~~ Distributions of this tagged sample are then fit to template shapes to extract the tagging efficiency and purity, both using simulation and data-driven techniques. The tagged jet spectrum is then corrected by the ~~distribution in data. The efficiency~~

of the charm tagger is found in simulation and is cross-checked by creating templates of the so called "Jet Probability", which is related to the probability that the individual tracks that make up the reconstructed jet are not associated to the primary vertex. The purity and efficiency values are then applied to the tagged distribution to obtain the c efficiency and purity to obtain the true charm jet spectrum and fraction.

2 Data and MC samples

2.1 Data sample

This analysis uses three different datasets including 35 nb^{-1} of pPb collisions at $\sqrt{s_{NN}}$ = 5.02 TeV and 4.8 pb^{-1} of pp collisions at $\sqrt{s}$ = 2.76 TeV collected by the CMS experiment during the 2013 heavy-ion heavy ion run period at the LHC, as well as 27.9 pb^{-1} of pp collisions at $\sqrt{s}$ = 5.02 TeV collected during the 2015 heavy-ion heavy ion run period. This analysis closely follows the event selections of previous pPb analyses and uses the same calibrations and corrections for the pPb data [8–10]. Five In addition to the event selections, a combination of jet triggers with varying energy thresholds was also perfomed. In the pPb analysis, five single-jet triggers with p_{T} thresholds of 20, 40, 60, 80, and 100 GeV/c^2 are combined in order to maximize statistics over a wide range of jet transverse momentum. This procedure trigger combination is also used in the analysis of b jets in pPb [8] and is described briefly here. In essence, the jet with the largest online raw jet p_{T}, i.e. the p_{T} used by the triggers before jet energy corrections, is used to classify each event. Based on the online raw jet p_{T}, it is possible to deduce which trigger(s) should have been fired by the jet. , irrespective of whether an additional artificial trigger rejection was applied to save disk space. This added rejection factor of a trigger is known as the prescale factor. If the highest threshold trigger that ought to have fired does indeed fire, the event is kept and weighted by the prescale value of that trigger trigger prescale factor, else the event is discarded.

For the 5.02 TeV pp data, the trigger menu was slightly altered in preparation for the higher instantaneous luminosity achieved in the 2015 run period, so only four triggers are combined with thresholds of 40, 60, 80, and 100 GeV/c^2. Due to jet energy smearing effects from reconstruction and resolution unfolding, the absence of a 20 GeV/c^2 trigger effectively places a 55 GeV/c lower bound on the leading jet p_{T} for the 5.02 TeV data.

2.2 MC sample

This analysis relies on simulations of pp collisions at 2.76 and 5.02 TeV, as well as simulations of pPb collisions at 5.02 TeV. Monte Carlo simulations of inclusive QCD hard-scattering events are generated using PYTHIA, version 6, tune Z2 [11], both at 2.76 and 5.02 TeV. These events are generated in phase space windows of the transverse momentum of the hard-scattering subprocess ($\hat{p}_T$) in order to expedite the production of jets with high transverse momentum. In order to properly build templates, unfold the jet resolution, and calculate tagging efficiency in the proton-nucleus environment, minimum-bias pPb events are produced using the HIJING event generator, version 1.383 [12] at 5.02 TeV. Then, inclusive QCD hard scattering events generated by 5.02 TeV PYTHIA 6 at 5.02 TeV events are embedded into each pPb background event. In this way, each pPb event contains at least one jet produced by a hard scattering process while still accurately representing the jet resolution and energy scale in a pPb environment.

During the pPb run, the proton and lead beams were run asymetrically in beam energy and therefore there is a center-of-mass pseudorapidity (η) shift of 0.465 units with respect to the laboratory frame. In addition, after 20.9 nb^{-1} of data was collected, the directions of the proton

and lead beams were reversed. To maintain consistency, this analysis defines the laboratory and the center-of-mass pseudorapidity such that $\eta_{\text{lab}} = \eta_{CM} + 0.465$, ~~or, rather,~~ which means that the proton beam direction is always defined to be in the positive-going direction. To account for resolution differences between the two boost directions, a MC production campaign was obtained for each beam direction. Of course, for the pp data, $\eta_{\text{lab}} = \eta_{CM}$.

3 The CMS detector and event selection

The CMS detector has excellent capabilities to perform displaced jet identification (b & c tagging) as demonstrated in Ref. [13]. The central feature of the CMS apparatus is a superconducting solenoid of 6 m internal diameter, providing a magnetic field of 3.8 T. Within the solenoid volume are a silicon pixel and strip tracker, a lead tungstate crystal electromagnetic calorimeter (ECAL), and a brass and scintillator hadron calorimeter (HCAL), each composed of a barrel and two endcap sections. The tracker has a pseudorapidity coverage of $|\eta_{\text{lab}}| < 2.4$, while the calorimetry covers $|\eta_{\text{lab}}| < 3$. Muons are measured in gas-ionization detectors embedded in the steel flux-return yoke outside the solenoid. Extensive forward calorimetry complements the coverage provided by the barrel and endcap detectors. A more detailed description of the CMS detector, together with a definition of the coordinate system used and the relevant kinematic variables, can be found in Ref. [14].

Event selections for this analysis are identical to previous pPb analyses [8–10] and include the requirement of a good primary vertex within 15 cm of the nominal interaction point and selections based on a HCAL noise cleaning filter. Beam-related background is suppressed by rejecting events in which less than 25% of all reconstructed tracks are of good quality.

Jets are reconstructed offline using the particle-flow algorithm, which identifies each individual jet constituent as one of a number of different particle types, including photons, electrons, muons, charged hadrons, and neutral hadrons. This is done using an optimized combination of information from the various elements of the CMS detector [15]. Jets are clustered by the anti-k$_T$ algorithm [16] with a size parameter of 0.3. Jet energy corrections are derived from simulation and using measurements of energy balance in dijet and photon+jet events. Jet momentum is found from simulation to be within 5% of the true jet momentum over the whole p_{T} spectrum and detector acceptance.

As jet energy corrections are only valid starting from 20 GeV/c, single jets are required to have a raw online $p_{\text{T}} > 20$ GeV/c and a fully-corrected $p_{\text{T}} > 35$ GeV/c. Jets in pp and pPb collisions are selected to correspond to an identical center-of-mass pseudorapidity window, namely $|\eta_{CM}| < 2$.

4 Charm tagging

A charm jet (c jet) is defined at generator level as any jet containing a prompt charm quark within the jet cone, that is, ignoring jets which contain a b→c cascade. Identification of such jets is achieved by tagging decays of charmed hadrons. This is difficult to achieve in practice as the $c\tau$ of such charmed hadron decays is only on the order of 100 μm. At CMS, the presence of a silicon tracker very close to the interaction point allows for the discrimination of secondary vertices with such minimal displacement values.

This c jet analysis closely follows previous analysis strategies for heavy-flavor jet tagging, namely the identification of b quark jets in heavy ions from CMS, both in lead-lead (PbPb) collisions [7] and pPb collisions [8]. This analysis strategy uses two discriminators to iden-

tify c jets. The first tagger uses reconstructed displaced vertices and is known as the Simple Secondary Vertex (SSV) tagger [13]. While the "high-efficiency" version of the tagger requires only vertices with two or more associated tracks, the version used in this analysis is the "high-purity" (SSVHP) version of the tagger and it requires that the secondary vertex has at least three associated tracks. Both versions require that all secondary vertices share less than 20% of tracks with any other vertex. The inclusion of the third associated vertex track in the high-purity version of the tagger allows for the selection of a working point that reduces the mistag rate of light jets by a factor of three, while still keeping the great majority of c jets, as shown in Fig. 1. With a reduced light jet contamination, c jets begin to dominate small regions of kinematic phase space, which this analysis exploits to extract relative flavor contributions of light, c, and b jets to the total jet sample.

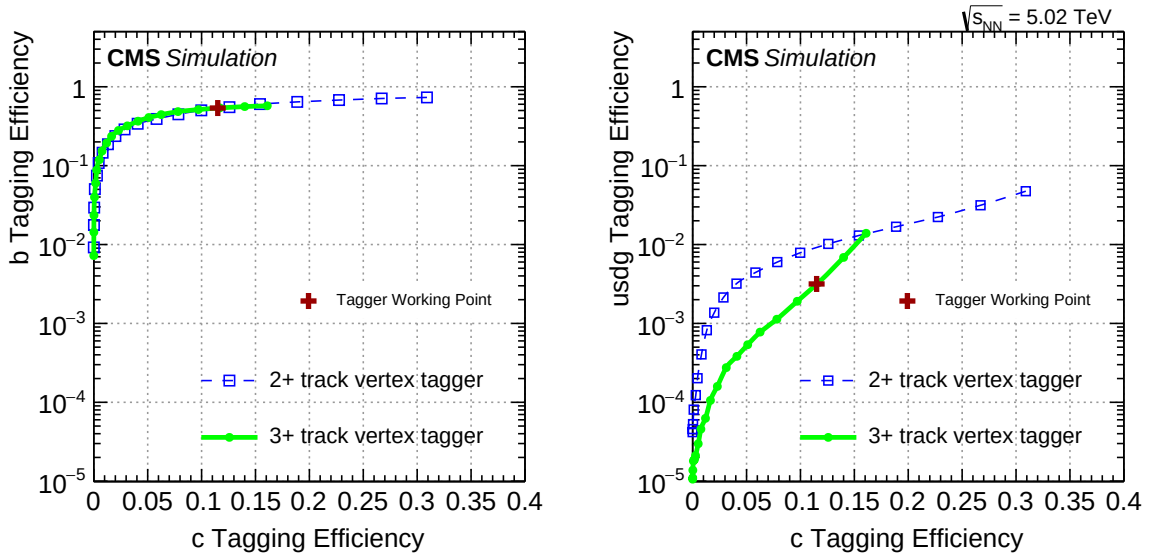

Figure 1: Efficiency curves are plotted for the high-purity (3+ track), and high-efficiency (2+ track) versions of the simple secondary vertex (SSV) tagger for both b jets (left) and light jets (right) as a function of c jet tagging efficiency. The charm-to-bottom discrimination power is virtually unchanged between the high-efficiency and high-purity versions of the tagger, while the light jet mistag rate is reduced by a factor of three at the analysis working point, shown as the closed red cross on the plot.

The second tagger used in this analysis is known as the Jet Probability (JP) tagger [13], and is used to cross-check the tagging efficiency predicted by simulation via a data-driven method. This tagger uses a discriminator based on single tracks that are significantly displaced from the primary vertex, and is therefore independent of secondary vertex reconstruction performance. The efficiency of a particular tagger (e.g. SSVHP) can be calculated with the JP tagger:

$$\epsilon_{\text{tag}} = \frac{C_c f_c^{\text{tagged}} N_{\text{jets}}^{\text{tagged}}}{f_c^{\text{pretag}} N_{\text{jets}}^{\text{pretag}}} \tag{1}$$

where f_c^{tagged} is the purity of the sample from a JP discriminator template fit after applying the SSVHP discriminator selection, f_c^{pretag} is the same before applying the SSVHP selection, $N_{\text{jets}}^{\text{pretag}}$ and $N_{\text{jets}}^{\text{tagged}}$ denote the number of jets before and after tagging, respectively, and C_c denotes the

fraction of jets that can be identified by the JP tagger (generally very close to 1).

The c jet purity calculation relies on another discriminating variable known as the corrected secondary vertex mass. This was first developed as an identifying tool for b jets by the experiments at LEP and SLAC [17] and is also used by the LHCb Collaboration [18]. The motivation behind this variable is to correct for the missing mass from the decay vertex due to neutral or otherwise unobserved particles. If the momentum vector of a vertex is not parallel to the vector pointing from the primary vertex to the secondary vertex decay point, i.e. the flight direction of the vertex, one can use conservation of transverse momentum to calculate a minimum possible mass the vertex must have had. This minimum possible mass is called the corrected secondary vertex mass "M_{corr}" and is defined as:

single

$$M_{\mathrm{corr}} = \sqrt{M^2 + p^2 \sin^2\theta} + p \sin\theta \tag{2}$$

where M is the invariant mass and p is the momentum of the vector sum of the reconstructed particles that form the secondary vertex and the angle θ is defined as the angle between that vector sum and the flight direction of the vertex. If all particles that belong to a given secondary vertex are reconstructed, the angle θ should be zero, and the secondary vertex mass needs no correction. Otherwise, additional mass-energy is added to the vertex to account for the non-reconstructed energy.

The c jet purity is found using template fits of M_{corr}, after tagging on the SSVHP (3+ track ~~) tagger, with a working point selection in pPb and pp collisions of SSVHP $>$ 1.68, which maximizes the estimated c jet purity from MC samples~~vertex) tagger. The numerical values of the SSV discriminator are correlated to the significance of the secondary vertex displacement with respect to the primary vertex and ~~is~~ are obtained using the formula: $\ln(1 + |d|/\sigma(d))$, where d is the three-dimensional vertex displacement and $\sigma(d)$ is the uncertainty on the displacement measurement. The working point used in this analysis requires SSVHP $>$ 1.68, which maximizes the estimated c jet purity from the MC samples. Once the working point is applied to the sample, distributions of corrected secondary vertex mass from light, c, and b jets in the PYTHIA+HIJING or PYTHIA simulations are fit to the distribution in data. The shapes of the different flavor templates are fixed, but the relative normalizations of each flavor is allowed to float independently. As seen in Fig. 2 for pPb collisions, and in Fig. 3 for pp collisions at 5.02 TeV, b jets dominate above 3 GeV/c^2, while the light jet contribution is significantly reduced by the SSVHP tagger requirement. Because of this light jet removal, the relative c jet contribution to the sample below 3 GeV/c^2 is quite large, allowing for an accurate extraction of the c jet purity in the data sample.

Once the purity is obtained via the template fits, the efficiency of the c tagging requirement (SSVHP $>$ 1.68) is calculated both from simulation and using distributions of the JP tagger [13] both before and after imposing the SSVHP tagging requirement. A unique advantage of using the JP tagger for calculating tagging efficiency via Eq. (1) is that it can be calibrated using data. By assuming that the track impact parameter resolution is independent of the presence of a jet, tracks with negative values of impact parameter significance (i.e. tracks with vertex displacements on the away-side of the vertex from the jet) can be used to compute a probability for the association of any given track to the primary vertex. The tagger distributions are calibrated such that the distribution of negative impact parameter is flat as a function of track displacement. The difference between the tagging efficiency from simulation and from the JP calculation is used in the systematic uncertainty estimation.

~~The~~ Figures 4 and 5 show the c tagging purity of the sample after applying the SSVHP tagger

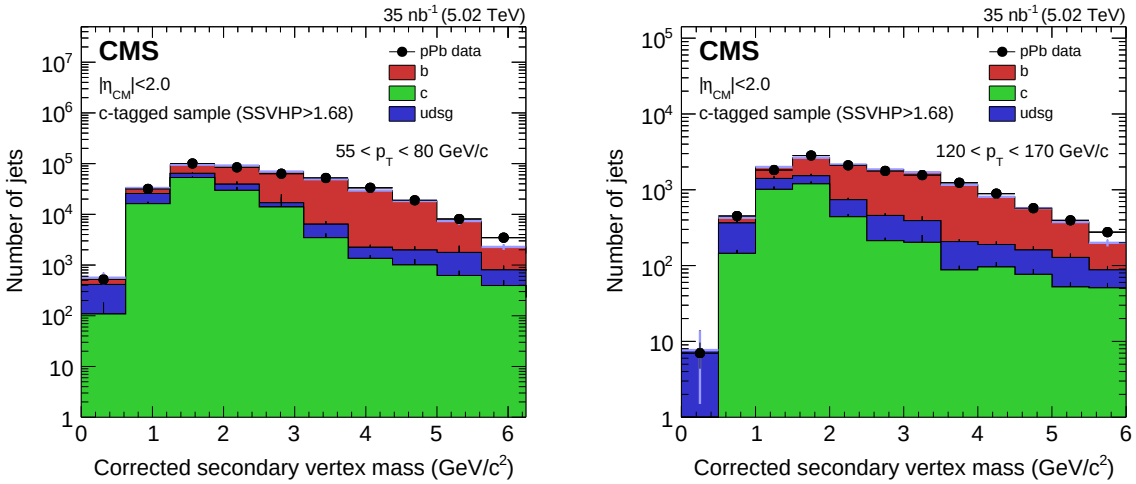

Figure 2: Distributions of corrected secondary vertex mass are plotted from PYTHIA+HIJING for c jets (green), light jets (blue), and b jets (red) in two example p_T bins. Relative normalizations of these three distributions are fit to a distribution from pPb collisions (black). Statistical uncertainties are shown in ~~green and~~ black~~for MC and data, respectively~~.

selection ~~is shown~~ for both simulation and data on the left, while the c tagging efficiency is shown for both simulation and data on the right~~in Figs. 4 and 5.~~. Figure 4 shows the distributions for 5.02 TeV pPb collisions, while Fig. 5 shows distributions for 5.02 and 2.76 TeV pp collisions.

Once the efficiency and purity values are obtained, the total number of c jets in the sample is obtained

$$N_{\text{cjets}} = N_{\text{jets}}^{\text{tagged}} \frac{f_c}{\epsilon_{\text{tag}}} \tag{3}$$

where $N_{\text{jets}}^{\text{tagged}}$ is the number of jets passing the SSVHP working point selection, f_c is again the c jet tagging purity, and ϵ_{tag} is the tagging efficiency. In addition, the tagged c jet sample is corrected by the purity and efficiency factors to obtain a c jet p_T spectrum. This spectrum is then passed through a Singular Value Decomposition (SVD) [19] unfolding procedure, as implemented by the ROOUNFOLD [20] package to remove the jet resolution effects.

5 Systematics and cross checks

Systematics for this analysis are divided into two primary categories: charm tagging and jet reconstruction.

5.1 Tagging systematics

A number of systematic checks on the charm-tagged spectrum are considered, including varying the SSVHP working point from 1.2 to 2.4, calculating ~~of~~ the c tagging efficiency using the JP tagger method instead of obtaining the value from simulation, varying ~~of~~ the gluon splitting fraction in the MC sample by 50% up and down, varying ~~of~~ the MC templates within their statistical uncertainties, and finally reweighting and varying the D meson decay parameters within their world-averaged uncertainties in the simulation.

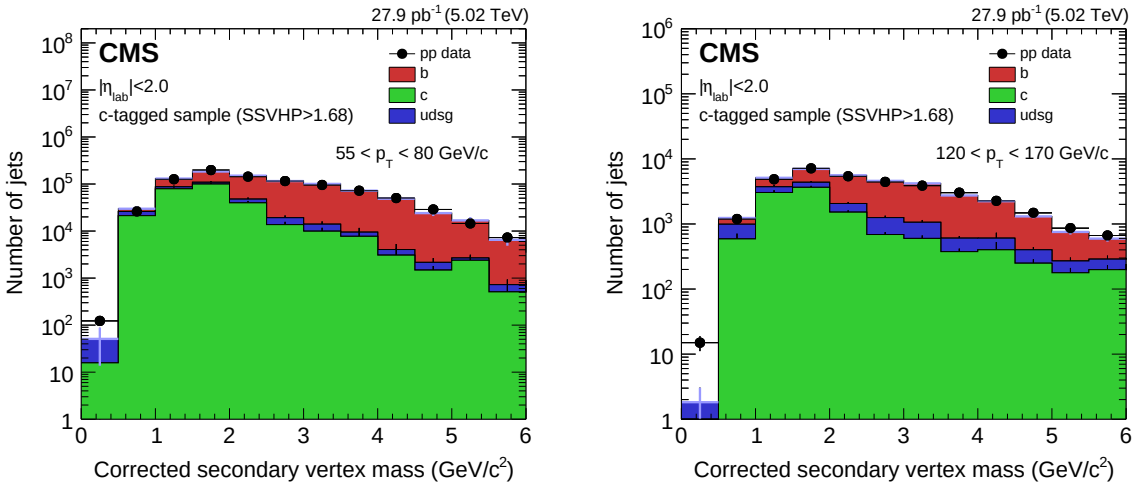

Figure 3: Distributions of corrected secondary vertex mass are shown from a PYTHIA 6, tune Z2 simulation for c jets (green), light jets (blue) and b jets (red) in two example p_T bins. Relative normalizations of these three distributions are fit to a distribution from pp data (black). Statistical uncertainties are shown in green and black for MC and data, respectively.

The tagger working point is varied over the discriminator working point region where the use of a discriminator enhances the c jet purity. With a very loose discriminator selection, the c jet purity is effectively unchanged from its value without a discriminator, while a very tight selection removes the great majority of both light and c jets such that the b jets dominate the sample. There is a narrow window in which the c jet purity is larger than in an unbiased sample, corresponding to SSVHP discriminator values between 1.2 and 2.4. To account for tagging fluctuations driven by tagger performance, we vary the working point of the tagger in steps of 0.2 units over this range and calculate the effective standard deviation from all working point variations. This leads to a 5-10% uncertainty, depending on jet p_T.

Next, an uncertainty is derived from the difference between the tagging efficiency as obtained from simulation and via fits to the JP tagger discriminator from Eq. (1). This accounts for a 5-10% uncertainty also as a function of p_T.

One of the primary theoretical unknowns in heavy-flavor jets is the impact of higher-order production, like gluon splitting, and how these effects manifest themselves in these fits. To account for this, the gluon splitting fraction in simulation is varied by 50% up and down and the distributions of corrected secondary vertex mass are refit to the modified MC templates, where both g→cc and g→bb splitting events are considered. This is a small but significant effect in both pPb and pp collisions ($< 5.5\%$).

The template statistical uncertainty is accounted for by varying the distributions of light, c, and b jets from MC within their statistical uncertainties using a toy MC study. The uncertainty is estimated by fitting the fluctuations in purity to a gaussian distribution, where the gaussian width is used as the uncertainty value. These values are ~~weakly~~ p_T-dependent, ranging from 5% at intermediate p_T to around 10% at low and high p_T.

Next, this analysis accounts for the possibility that the PYTHIA simulation does not accurately reproduce the D meson decay kinematics. Since we require a secondary vertex that decays into at least three particles to tag jets, we study the influence of the D meson decay parameters by reweighting both the relative D meson branching ratios and the D meson fragmentation

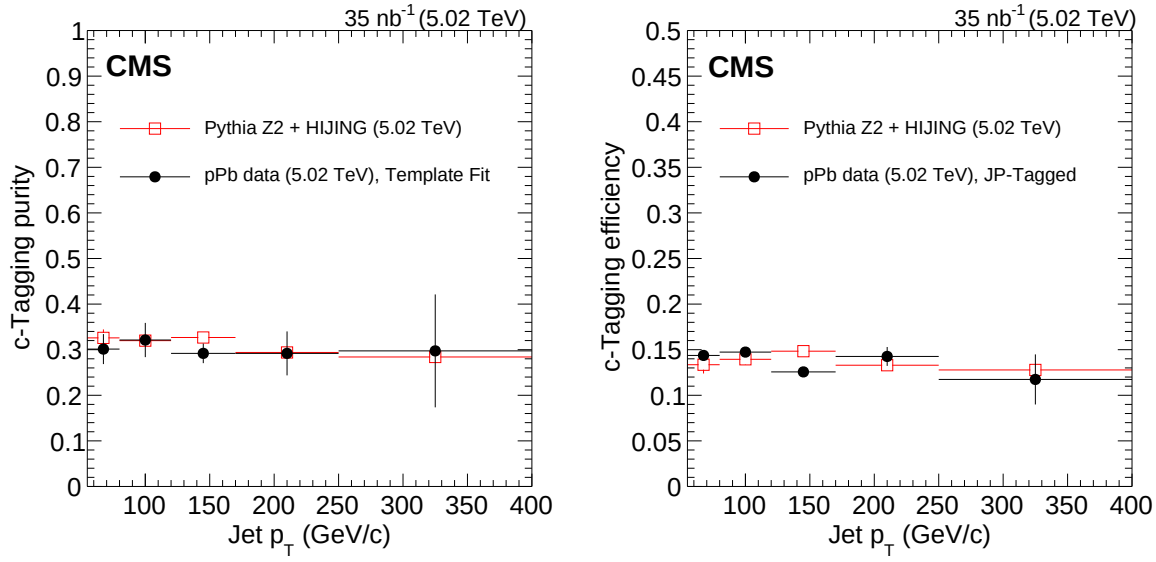

Figure 4: The tagging purity (left) and efficiency (right) for the working point selection of SSVHP > 1.68 in pPb collisions at 5.02 TeV. Purity curves from MC (red) and data (black) are shown, obtained by fitting templates to data, along with efficiency curves from MC (red) and the JP cross-check (black).

in simulation to match the world-averaged values from previous experiments. We find that reweighting and varying these values within their uncertainties leads to a 5.5% effect, independent of jet p_{T}.

The contributions from each source of systematic uncertainty are ~~quadratically summed~~ summed in quadrature to obtain an overall systematic uncertainty from ~~c-jet~~ c jet tagging. When summed, these tagging uncertainties lead to a 12-15% uncertainty on the c jet fraction in pPb collisions, and a 10-12% uncertainty ~~on the same~~ in pp collisions~~below 250 . The result from 2.76 TeV pp collisions above 250 has an 80tagging uncertainty due to lack of statistical precision, so this point is omitted from the result plots.~~ .

5.2 Jet reconstruction systematics

Additional uncertainties stem from basic jet reconstruction. Jet energy corrections are derived from simulation samples and via energy balance measurements with photon+jet events and have an uncertainty due to the jet resolution of about 5%, while the jet energy scale uncertainty ranges from 2-3%, depending on p_{T} and η. In addition, the SVD unfolding is cross-checked by comparing to alternative unfolding methods, including Bayesian unfolding, and by varying the prior "truth" spectrum from simulation. ~~This accounts for a~~ The uncertainty on the unfolding procedure is around 5%~~and~~ , while a 4% uncertainty ~~, respectively~~is quoted due to the uncertainty on the simulation "truth" spectrum shape. Together, all these reconstruction-based uncertainties are added in quadrature and total between 12-15% in pPb collisions and around 15% in pp collisions. Finally, the luminosity measurement of the pPb data has an uncertainty of 3.6%, while the luminosity measurement ~~uncertainty~~ uncertainties in pp data at 2.76 TeV and 5 TeV ~~is~~ are 3.7% and 3.6%, respectively. As the uncertainties from the jet energy resolution, unfolding, and the prior "truth" spectrum are cancelled in the c jet fraction measurement, they are applied only to the cross-section measurement.

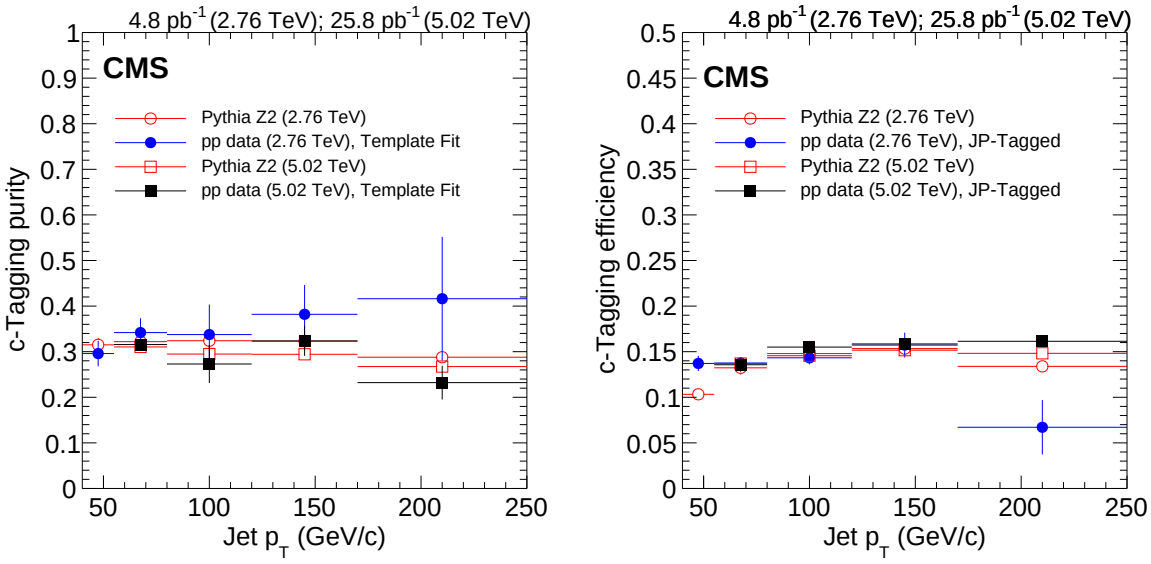

Figure 5: The tagging purity (left) and efficiency (right) for the working point selection of SSVHP > 1.68 in pp collisions at 5.02 TeV (square markers) and at 2.76 TeV (circular markers). Purity curves from MC (open red markers) and data (closed black markers) are shown, obtained by fitting templates to the data. The right plot shows efficiency curves from MC (open red markers) and the JP-tagged data-driven cross-check (closed ~~black~~ markers).

6 Results

The c jet spectra in pp collisions ~~is~~ are shown in Fig. 6 for 5.02 ~~TeV collisions~~ (left) and ~~for~~ 2.76 ~~TeV collisions~~ (right) ~~.~~ TeV collisions. The spectra from data are corrected for jet resolution by a SVD unfolding procedure as implemented by the RooUnfold package. Both spectra are compared to a prediction from the Z2 tune of Pythia 6. The bottom panels of Fig. 6 ~~shows~~ show the c jet fraction in pp for both collision energies. A comparison of the two c jet fractions at 2.76 ~~TeV~~ and 5.02 TeV suggests that the collision energy dependence of the c jet fraction is small and is well within systematic uncertainties. In addition, data at both energies conform to predictions from the Pythia simulations.

The c jet spectrum as a function of p_{T} is shown in the top panel of Fig. 7 ~~in~~ for pPb and pp collisions at 5.02 TeV. The spectra ~~from data are corrected for jet resolution by a SVD unfolding procedure as implemented by the RooUnfoldpackage. The spectra are then~~ are normalized by the total integrated luminosity of the sample. ~~In addition, the~~ The pPb c jet spectrum is also scaled by the mass number of lead (A=208) ~~multiplied by the minimum bias~~ divided by the minimum-bias cross-section ~~in pPb divided by that in pp~~for pPb collisions. This total factor is known as T_{pA} and is the effective enhancement of jet production due simply to geometrical effects in pPb, as predicted by the Glauber model [21]. This additional scaling allows for a direct comparison of the pPb data to the pp data at the same center-of-mass energy. The direct comparison is known as the R_{pA} value, which is defined in general as:

$$R_{\mathrm{pA}} = \frac{1}{T_{\mathrm{pA}}} \frac{dN^{\mathrm{pPb}}}{dp_{\mathrm{T}}} \Big/ \frac{d\sigma^{\mathrm{pp}}}{dp_{\mathrm{T}}} \tag{4}$$

In the bottom panel of Fig. 7, the c jet R_{pA} value is calculated at 5.02 TeV. We observe ~~a~~ an

R_{pA} value consistent with unity, suggesting that initial state nuclear modification effects are small for c jets at large values of transverse momentum, confirming pQCD predictions indicating such behavior. Fitting a constant to the pPb c jet R_{pA} gives a measurement of 0.951 $\pm$ 0.139 (stat+syst) $\pm$ 0.04 (lumi).

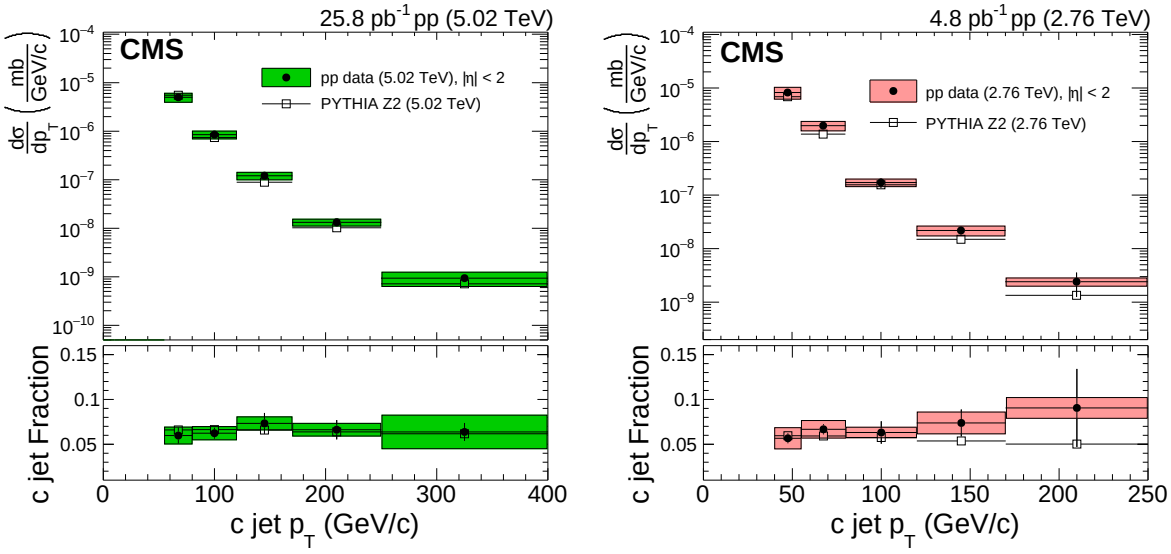

Figure 6: The c jet spectra for 5.02 TeV pp data is shown on the left top panel, compared to a PYTHIA 6 prediction. The lower panel shows the c jet fraction as a function of jet p_T for both pp data and PYTHIA. The right figure shows the same but for pp data at 2.76 TeV, along with a PYTHIA comparison to data. Systematic errors are shown as filled colored boxes.

7 Summary

~~Results presented here show that it is possible to identify jets from charm quark decays in collision environments with a nucleus~~Transverse momentum spectra for charm quark jets have been obtained for pPb collisions at $\sqrt{s_{NN}}$ = 5.02 TeV as well as for pp collisions at $\sqrt{s}$ = 2.76 and 5.02 TeV. We observe ~~an~~ a p_T-independent R_{pA} value of 0.951 $\pm$ 0.139 (stat+syst) $\pm$ 0.04 (lumi) for c jets at 5.02 TeV, indicating that no significant jet energy modification is present in pPb collisions for c jets with transverse momenta above 55 GeV/c. In addition, we observe that the c jet fraction is consistent with PYTHIA predictions for ~~both pPb and~~ pp collisions at ~~both~~ center-of-mass energies of 2.76 and 5.02 TeV. These measurements indicate that proton-lead initial state effects on charm quark jets above 55 GeV/c are quite small and future measurements of charm jet quenching in lead-lead collisions will not be affected by such effects.

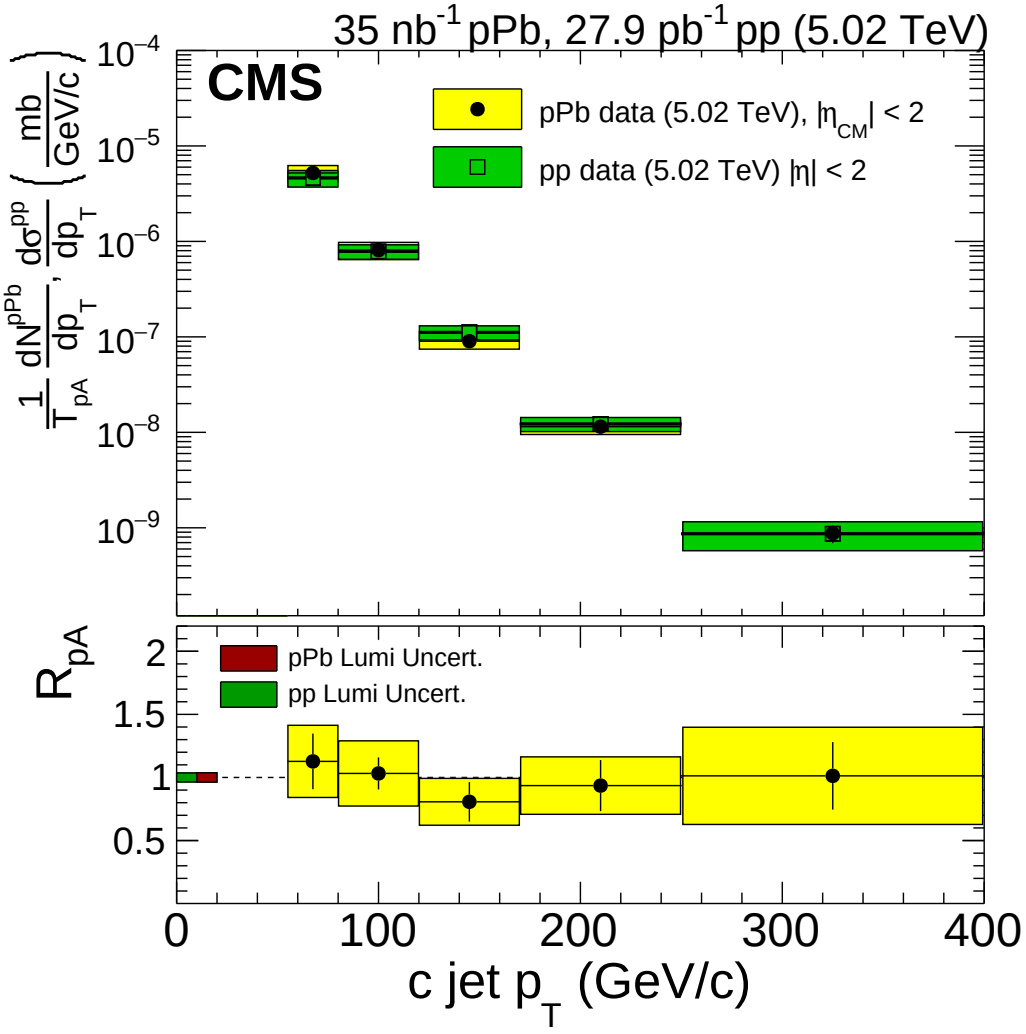

Figure 7: The top panel shows the c jet spectrum for 5.02 TeV pPb and pp data, while the bottom panel shows the c jet R_{pA} at 5.02 TeV. Systematic errors are calculated for the data and are shown as solid yellow bands around the R_{pA} values. Luminosity uncertainties are also shown for pp and pPb.

References

[1] J. D. Bjorken, "Energy loss of energetic partons in QGP: possible extinction of high p_T jets in hadron-hadron collisions", *FERMILAB-PUB-82-059-THY* (1982).

[2] C.A. Salgado, et. al., "Proton-Nucleus Collisions at the LHC: Scientific Opportunities and Requirements", *J. Phys. G.* **39** (2012) 015010, doi:10.1088/0954-3899/39/1/015010, arXiv:1105.3919.

[3] H. van Hees, R. Rapp, "Thermalization of Heavy Quarks in the Quark-Gluon Plasma", *Phys. Rev. C* **71** (2005) 034907, doi:10.1103/PhysRevC.71.034907, arXiv:nucl-th/0412015.

[4] G.D. Moore, D. Teaney, "How Much do Heavy Quarks Thermalize in a Heavy Ion Collision?", *Phys. Rev. C* **71** (2005) 064904, doi:10.1103/PhysRevC.71.064904, arXiv:hep-ph/0412346.

[5] D. d'Enterria, "Jet quenching", ch. 6.4. Springer Materials, 2010. arXiv:0902.2011. doi:10.1007/978-3-642-01539-7_16.

[6] J. Huang, Z. B. Kang, and I. Vitev, "Inclusive b-jet production in heavy ion collisions at the LHC", *Phys. Lett. B* **726** (2013) 251, doi:10.1016/j.physletb.2013.08.009, arXiv:1306.0909.

[7] CMS Collaboration, "Evidence of b-jet quenching in PbPb collisions at $\sqrt{s_{NN}}$ = 2.76 TeV", *Phys. Rev. Lett.* **113** (2014) 132301, doi:10.1103/PhysRevLett.113.132301, arXiv:1312.4198.

[8] CMS Collaboration, "Transverse momentum spectra of b jets in pPb collisions at $\sqrt{s_{NN}}$ = 5.02 TeV", *Phys. Lett. B* **754** (2016) 59, doi:10.1016/j.physletb.2016.01.010, arXiv:1510.03373.

[9] CMS Collaboration, "Nuclear effects on the transverse momentum spectra of charged particles in pPb collisions at a nucleon-nucleon center-of-mass energy of 5.02 TeV", *Eur. Phys. J. C* **75** (2015) 237, doi:10.1140/epjc/s10052-015-3435-4, arXiv:1502.05387.

[10] CMS Collaboration, "Measurement of inclusive jet nuclear modification factor in pPb collisions at $\sqrt{s_{NN}}$ = 5.02 TeV", *Eur. Phys. J. C* **76** (2016) 372, doi:10.1140/epjc/s10052-016-4205-7, arXiv:1601.02001.

[11] Rick Field, "Min-Bias and the Underlying Event at the LHC", *Acta Phys. Polon. B* **42** (2011) 2631, doi:10.5506/APhysPolB.42.2631, arXiv:1110.5530.

[12] X.-N. Wang and M. Gyulassy, "HIJING: A Monte Carlo Program for Parton and Particle Production in High Energy Hadronic and Nuclear Collisions", *Comp. Phys. Comm.* **83** (1994) 307, doi:10.1016/0010-4655(94)90057-4, arXiv:nucl-th/9502021.

[13] CMS Collaboration, "Identification of b-quark jets with the CMS experiment", *JINST* **8** (2013) P04013, doi:10.1088/1748-0221/8/04/P04013, arXiv:1211.4462.

[14] CMS Collaboration, "The CMS experiment at the CERN LHC", *JINST* **3** (2008) S08004, doi:10.1088/1748-0221/3/08/S08004.

[15] CMS Collaboration, "Particle-flow event reconstruction in CMS and performance for jets, taus, and $E_{\mathrm{T}}^{\mathrm{miss}}$", (2009). CMS-PAS-PFT-09-001.

[16] M. Cacciari, G. P. Salam, and G. Soyez, "The anti-k_t jet clustering algorithm", *JHEP* **04** (2008) 063, doi:10.1088/1126-6708/2008/04/063, arXiv:0802.1189.

[17] G. J. Barker, "b-quark physics with the LEP collider", *Springer Tracts Mod. Phys.* **236** (2010) 170, doi:10.1007/978-3-642-05279-8.

[18] LHCb Collaboration, "Identification of beauty and charm quark jets at LHCb", *JINST* **10** (2015) P06013, doi:10.1088/1748-0221/10/06/P06013, arXiv:1504.07670.

[19] V. K. Andreas Hoecker, "SVD Approach to Data Unfolding", *Nucl. Instr. Meth. A* **372** (1996) 469, doi:10.1016/0168-9002(95)01478-0, arXiv:hep-ph/9509307.

[20] T. Adye, "Unfolding algorithms and tests using RooUnfold", in *PHYSTAT 2011 Workshop on Statistical Issues Related to Discovery Claims in Search Experiments and Unfolding*, pp. 313–318. 2011. arXiv:1105.1160. doi:10.5170/CERN-2011-006.

[21] B. Alver, M. Baker, C. Loizides, and P. Steinberg, "The PHOBOS Glauber Monte Carlo", arXiv:0805.4411.